AD-A055 245 COLD REGIONS RESEARCH AND ENGINEERING LAB HANOVER N H F/G 8/12
A COMPARISON BETWEEN DERIVED INTERNAL DIELECTRIC PROPERTIES AND--ETC(U)
APR 78 T E KELIHER, S F ACKLEY

UNCLASSIFIED CRREL-78-4 NL

1 OF 1
AD
A055 245

END
DATE
FILMED
7-78
DDC

CRREL REPORT 78-4

A comparison between derived internal dielectric properties and radio-echo sounding records of the ice sheet at Cape Folger, Antarctica

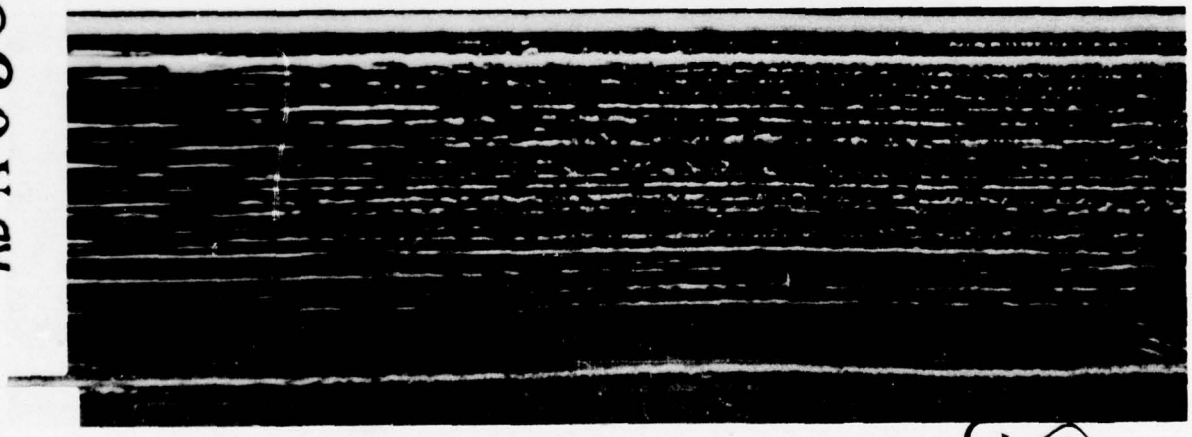

Cover: An airborne radio-echo sounding record, obtained using a 60-MHz sounder from the ice sheet in the vicinity of Byrd Station, Antarctica (80°S, 120°W). S and b represent the surface and bottom of the ice sheet, and the horizontal white lines between them are radar returns from internal layers within the ice sheet. The ice thickness of 2164 m measured by the core taken at this location is in good agreement with the radar computation using the travel/time scale below the photo and a velocity of radiowaves in ice of 168 m/μsec (two-way travel time). (This photo was provided by Dr. D.J. Drewry of the Scott Polar Research Institute, Cambridge, England.)

CRREL Report 78-4

A comparison between derived internal dielectric properties and radio-echo sounding records of the ice sheet at Cape Folger, Antarctica

T.E. Keliher and S.F. Ackley

April 1978

Prepared for
DIRECTORATE OF FACILITIES ENGINEERING
OFFICE, CHIEF OF ENGINEERS
By
CORPS OF ENGINEERS, U.S. ARMY
COLD REGIONS RESEARCH AND ENGINEERING LABORATORY
HANOVER, NEW HAMPSHIRE

Unclassified

SECURITY CLASSIFICATION OF THIS PAGE (When Data Entered)

REPORT DOCUMENTATION PAGE

READ INSTRUCTIONS BEFORE COMPLETING FORM

1. REPORT NUMBER: CRREL Report 78-4
2. GOVT ACCESSION NO.
3. RECIPIENT'S CATALOG NUMBER: CRREL-78-4
4. TITLE (and Subtitle): A COMPARISON BETWEEN DERIVED INTERNAL DIELECTRIC PROPERTIES AND RADIO-ECHO SOUNDING RECORDS OF THE ICE SHEET AT CAPE FOLGER, ANTARCTICA
5. TYPE OF REPORT & PERIOD COVERED
6. PERFORMING ORG. REPORT NUMBER
7. AUTHOR(a): T.E. Keliher, S.F. Ackley
8. CONTRACT OR GRANT NUMBER(a)
9. PERFORMING ORGANIZATION NAME AND ADDRESS: U.S. Army Cold Regions Research and Engineering Laboratory, Hanover, New Hampshire 03755
10. PROGRAM ELEMENT, PROJECT, TASK AREA & WORK UNIT NUMBERS: Project 4A161102AT24, Task A3, E1, Work Unit 002
11. CONTROLLING OFFICE NAME AND ADDRESS: Directorate of Facilities Engineering, Office, Chief of Engineers, Washington, D.C. 20314
12. REPORT DATE: April 1978
13. NUMBER OF PAGES: 18
14. MONITORING AGENCY NAME & ADDRESS (if different from Controlling Office): 20 p.
15. SECURITY CLASS. (of this report): Unclassified
15a. DECLASSIFICATION/DOWNGRADING SCHEDULE
16. DISTRIBUTION STATEMENT (of this Report): Approved for public release; distribution unlimited.
17. DISTRIBUTION STATEMENT (of the abstract entered in Block 20, if different from Report): 6 110 2A
18. SUPPLEMENTARY NOTES
19. KEY WORDS (Continue on reverse side if necessary and identify by block number): Antarctica; Dielectric properties; Ice sheets; Internal ice layers; Radio-echo sounding
20. ABSTRACT (Continue on reverse side if necessary and identify by block number)

The use of radio-echo sounding records to indicate the presence of internal layers within large ice sheets is of interest to glaciologists because it offers a means of tracking the internal properties of the ice sheets over large distances. The interpretation of the reflections obtained in this manner is more valuable, however, if a *physical* property change relating to the glaciological regime can be related to the *dielectric* property change producing the radio-echo reflections. In this report, we use the measured physical properties of core to bedrock taken at Cape Folger, East Antarctica (66°22'S, 111°E, 324-m depth), to compute a profile of dielectric properties and from this, a depth-reflection coefficient profile for comparison with the observed radio-echo reflections. The measurements available on physical

CONT →

DD FORM 1 JAN 73 1473 EDITION OF 1 NOV 65 IS OBSOLETE

Unclassified

SECURITY CLASSIFICATION OF THIS PAGE (When Data Entered)

(66 deg 22 min S,

037 100

20. Abstract (cont'd)

properties are: density variations, bubble size and shape changes, and crystal fabric variations. The depths of the strong reflections shown on the available radio-echo records are in reasonable agreement with the depths corresponding to the highest reflection coefficients computed from the combined physical property measurements. In calculations to differentiate the separate effects of different physical properties, it appears that density variations account for the primary contributions to the calculated dielectric property changes corresponding to the highest reflection coefficients. However, bubble changes alone can also account for reasonable, though lower, reflection coefficients at the appropriate depths. Crystal fabric variations correspond poorly with the reflection locations. Density variations are normally associated with depositional events in the history of the ice sheet. However, the close correspondence between the depths of the bubble shape changes (which are definitely deformational features), and the depths of the density variations, and between both of these and the radio-echo layers, indicates that deformational events in the ice sheet's history are represented by the variations in the physical property and associated radio-echo records.

ABSTRACT

PREFACE

This report was prepared by T.E. Keliher, Research Associate, Department of Meteorology, University of Melbourne, Parkville, Victoria, Australia, and S.F. Ackley, Research Physicist, Snow and Ice Branch, Research Division, U.S. Army Cold Regions Research and Engineering Laboratory (CRREL).

The study was conducted under DA Project 4A161102AT24, *Research in Ice and Frozen Ground;* Task A3, *Research in Terrain and Climatic Constraints,* E1, *Cold Environment Factors;* Work Unit 002, *Adhesion and Physics of Ice.*

Dr. Steven A. Arcone and Dr. Anthony J. Gow of CRREL reviewed the technical content of this report.

The authors thank Dr. W.F. Budd, Antarctic Division, Department of Science, Australia, for providing the unpublished data on ice core physical properties used in this report and for encouraging and supporting this work. Both of the authors also gratefully acknowledge the support of the Meteorology Department, University of Melbourne, Dr. U. Radok, Chairman, during this investigation. S.F. Ackley particularly acknowledges the support of CRREL.

CONTENTS

ILLUSTRATIONS

NOMENCLATURE

A_i	depolarization factor
a, b, c	diameters in x, y, z space of a general ellipsoid
d_i	thickness of layer i (meters)
f	radio frequency (Hz)
j	$\sqrt{-1}$
ℓ	thickness of an ash or dust layer
n	total number of layers
P	proportion of ash to ice in a layer
r_i	EM reflection amplitude of layer i
R	power reflection coefficient of mixture of ash and ice
R_i	power reflection coefficient of layer i
s	variable relating general ellipsoid to the "standard" ellipsoid
v_2	volume density of component 2
Z_i	bulk impedance of layer i
$\hat{Z}_i$	surface impedance equivalent to half-space impedance below layer i
γ_i	propagation constant of layer i
ϵ_0	permittivity of free space
ϵ_i	relative dielectric constant (to free space) of layer i
$\epsilon'(\omega)$	dielectric constant of a medium as a function of frequency
ϵ_1, ϵ_2	dielectric constants of the components 1 and 2 of a mixture dielectric
ϵ	total dielectric constant of the mixture
ϵ_a	dielectric constant of a mixture containing ellipsoids with E-field parallel to the "long" axis a
ϵ_b	dielectric constant of a mixture containing ellipsoids with E-field parallel to the "short" axis b
ϵ_{ab}	dielectric constant of a mixture containing ellipsoids with a random spatial orientation
ϵ_s	dielectric constant of a mixture containing spheres as the included second dielectric
ϵ_∞	dielectric constant at infinite frequency
$\Delta\epsilon_n$	contribution to the dielectric constant from polarization process n
$\epsilon_\perp$	dielectric constant of ice measured perpendicular to the c-axis
$\epsilon_{\parallel}$	dielectric constant of ice measured parallel to the c-axis
ϵ'	real part of the complex dielectric constant
ϵ''	imaginary part of the complex dielectric constant
θ	angle measured in the vertical between E-M propagation direction and crystal axis
λ	wavelength of the incident radiation
$\bar{\theta}$	mean vertical angle of the c-axis distribution

ϕ	azimuth angle of crystal axis
$\rho_L(z)$	linear regression of density upon depth
ρ_{ice}	density of ice
ρ_i	density of layer *i*
μ_0	magnetic permeability of free space (henrys/m)
σ_i	conductivity of layer *i*
τ_n	relaxation time of the polarization process *n*
ω_n	angular frequency (n) of the polarization process *n*
ω	angular frequency = $2\pi f$ (sec^{-1})
$\tan\delta$	loss tangent of a medium = ϵ''/ϵ'
$d\Omega$	$\sin\theta d\theta d\phi$
$n(\theta,\phi)$	percentage of ice crystals with crystal axes at angles θ, ϕ

A COMPARISON BETWEEN DERIVED INTERNAL DIELECTRIC PROPERTIES AND RADIO-ECHO SOUNDING RECORDS OF THE ICE SHEET AT CAPE FOLGER, ANTARCTICA

T.E. Keliher and S.F. Ackley

INTRODUCTION

The use of radio-echo sounding records to indicate the presence of internal layers within large ice sheets is of interest to glaciologists because it offers a means of tracking the internal properties of the ice sheets over large distances. The glaciological interpretation is difficult, however, because the cause of the internal layering is not clear. In fact, several physical causes for the dielectric changes of the ice producing internal reflections have been offered (Harrison 1973). Each of these causes is glaciologically significant, but in a different manner, so that large-scale internal layering within the ice cannot be unequivocally interpreted as a particular stratigraphic horizon relating to a chemical, deformational, or temperature-depositional characteristic of the ice. It is also possible that a single radar reflection may arise from the vector sum of reflections from several layers.

In this report we first review a computational method to obtain reflection coefficients (Linlor and Jiracek 1975) and next review several possible physical mechanisms that can produce the necessary dielectric constant variations leading to reflections. We then use the measured physical properties of the core to bedrock from Cape Folger near Casey Station, East Antarctica (66°20'S, 111°E; 324-m depth), to calculate the contribution to the dielectric property change with depth from each observed physical cause. From the calculated dielectric profile, we compute a derived power reflection coefficient-depth profile. We then compare this computed reflection coefficient profile, obtained from the individual and combined physical property changes of the ice, with the actual radio-echo sounding reflection profile in an effort to interpret the causes of the internal reflections.

DERIVATION OF THE POWER REFLECTION COEFFICIENT-DEPTH VARIATION

The power reflection coefficient is calculated in the following manner after Linlor and Jiracek (1975) and Wait (1958). The characteristic bulk impedance Z_i of layer i is defined by

$$Z_i = \frac{j\mu_0 \omega}{\gamma_i} \tag{1}$$

where $j = \sqrt{-1}$
μ_0 = magnetic permeability of free space
ω = angular frequency = $2\pi f$ (f in Hz)
γ_i = propagation constant.

Generally γ_i is a complex quantity defined by:

$$\gamma_i^2 = \epsilon_0 \mu_0 \epsilon_i \omega^2 + j\mu_0 \sigma_i \omega \tag{2}$$

where ϵ_0 = permittivity of free space
ϵ_i = relative lossless dielectric constant of the medium
σ_i = conductivity.

In our formulation the ice medium is considered lossless, so we only consider the real part of the propagation constant, or:

$$\gamma_i = \omega\sqrt{\epsilon_0 \mu_0 \epsilon_i} \ . \tag{3}$$

Paren and Robin (1975) have considered the effects of conductivity changes in ice sheets (corresponding to a change in the imaginary part of eq 2) on internal reflections but have indicated that these effects are significant at depths over 1000 m deeper than the core

considered here. We discuss this aspect further in a later section.

The reflection *amplitude* r_i at a boundary within the medium is given by

$$r_i = \frac{Z_{i-1} - \hat{Z}_i}{Z_{i-1} + \hat{Z}_i} \tag{4a}$$

and the reflection *power* (what is detected by the receiver) is

$$R_i = r_i^2. \tag{4b}$$

Z_{i-1} is the characteristic bulk impedance of the $i-1$st layer as defined above, while $\hat{Z}_i$ is the surface impedance of the ith layer and, after Wait (1958), is defined by

$$\hat{Z}_i = Z_i \frac{\hat{Z}_{i+1} + Z_i \tanh \gamma_i d_i}{Z_i + \hat{Z}_{i+1} \tanh \gamma_i d_i}. \tag{5}$$

Here, d_i = the thickness of layer i and γ_i = the propagation constant as given above. The bottom or nth layer at bedrock is taken to be semi-infinite and therefore

$$\hat{Z}_n = Z_n. \tag{6}$$

The procedure to obtain the estimated reflection coefficient profile with depth is to "build up" the ice sheet from the bottom, layer by layer, using some estimate of the propagation constant based on the ice properties at each depth. The bulk impedance of a layer is calculated from eq 1. Eq 5 is then used with the calculated bulk impedance, estimated propagation constant and estimated layer thickness to obtain the surface or input impedance of the top which replaces the "layered" dielectric below by a homogeneous half space with equivalent surface impedance.

The variation of reflection coefficient with depth, which is the source of internal reflections within the ice sheet, is therefore dependent on the "mismatch" in impedance between the bulk impedance of the layer under study and the surface impedance of the half-space below the layer. From eq 1 and 5 we see that these two quantities are dependent only on the dielectric constant and thickness of the layers for a given radar wavelength.

POSSIBLE SOURCES OF DIELECTRIC CONSTANT VARIATION WITH DEPTH IN ICE SHEETS

In this analysis one effect we do not consider is the contribution of interference between reflected waves

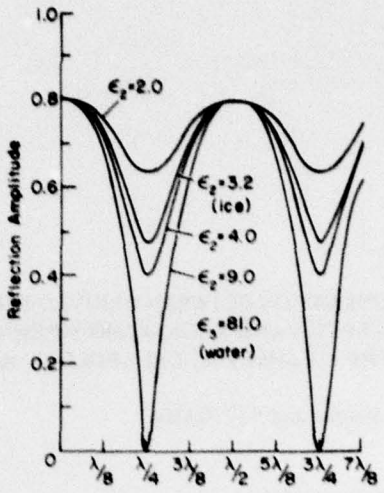

Figure 1. Reflection amplitude as a function of layer thickness measured in wavelength of the incident wave (after Linlor and Jiracek 1975). As shown here, the curves represent an ice sheet floating on water. Similar curves can be generated for analogous 3-layer media [e.g., air-snow/ice-bedrock (as discussed here)].

to the observed reflections within ice sheets. When the thickness of a layer is either an even or an odd multiple of a quarter wavelength of the incident wave, constructive or destructive interference occurs between two reflected waves. The reflected power can then be enhanced or reduced if a layer thickness is at the quarter wavelength multiple value. To accurately evaluate this effect is beyond the resolution of the currently available data on the physical properties of the ice. The quarter wavelength phenomenon would not, a priori, be expected to be highly probable since it demands an accurate match of input wavelength with the particular layer thickness in the ice sheet.

In the future, a simple test on whether a reflection occurs or disappears because of a match between the wavelength and layer thickness could be simply performed by sounding at two slightly different frequencies, since the reflection amplitude changes quite rapidly with a slight mismatch between the layer thickness and the quarter wavelength, as shown in Figure 1 (after Linlor and Jiracek 1975). Therefore, if the quarter wavelength – thickness match were a factor, the reflected power from the layer under consideration would be markedly different at the two frequencies, while it would not change significantly if the quarter wavelength phenomenon were absent. Because internal reflections have been noted since the advent of radio-echo sounding

at frequencies varying from 30 MHz to the GHz range, we assume initially that the observed echoes are derived from depth changes in ice dielectric properties (leading to a change in impedance with depth as given in eqs 1, 2, and 5) rather than from a fortuitous coincidence of layer thickness and quarter wavelengths.

The possible mechanisms for dielectric variations in ice sheets will be briefly reviewed here. The mechanisms mentioned have been (i) ice density variations (Robin et al. 1969), (ii) macroscopic impurity layers [dust and volcanic ash (Robin et al. 1969)], (iii) microscopic impurity layers (Paren and Robin 1975), (iv) a previously unstudied effect for this application, changes in air bubble geometry from spherical to ellipsoidal shapes, and (v) crystal orientation changes (Harrison 1973). Except for microscopic impurity variations, all of these give rise to small changes in dielectric permittivity, or the real part of the dielectric constant.

Ice density variations

The ice density variation is given as (Gudmandsen 1971)

$$\sqrt{\epsilon'} = 1 + 0.85\,\rho_i. \tag{7}$$

The variation in dielectric constant with density arises from the mixture of two media, air and ice, with different dielectric constants, ($\epsilon_{air} = 1$, $\epsilon_{ice} = 3.17$). The density relationship (eq 7) is empirical, based on a fit to experimental data (Robin et al. 1969). The ice density variation and the effect of macroscopic impurities are specific examples of a more general treatment for any geometric dielectric inclusion, which we discuss later.

***Effect of macroscopic impurity layers* (dust and volcanic ash)**

The effect of these layers, arising from the fallout of volcanic eruptions, is similar to the effect described above for density; namely, the dielectric constant of a mixed ice and ash/dust layer will be a function of the dielectric constants of ice (3.17) and of ash (e.g., 4.8) and the relative proportions of the two components. After Robin et al. (1969), the power reflection coefficient of a mixture of ash and ice R contained in a layer of thickness ℓ is

$$R = (0.4\,\pi P \ell/\lambda)^2 \tag{8}$$

where P = proportion of ash to ice (P:1)
ℓ = layer thickness
λ = wavelength.

An example at the wavelength corresponding to 35 MHz indicates layers 1 and 5 cm thick containing 10% ash would have reflection coefficients of – 74 dB and – 60 dB, which are within the observable range for most current echo sounding receivers. Ash layers have been observed at several locations within the deep core obtained at Byrd Station, Antarctica (Gow and Williamson 1971), although the thicknesses are lower than those of the above example, of the order of 0.05 cm at 10% concentration.

Effect of microscopic impurity layers

Paren and Robin (1975) argue that, as well as the changes in the real part of the dielectric constant given by eqs 3 and 4, there is also an impedance mismatch caused by variations in the conductivity or loss tangent, $\tan\delta$, of the ice ($\tan\delta = \epsilon''/\epsilon'$ where ϵ'', the imaginary part of the dielectric constant $= \sigma/\omega\epsilon_0$). In their formulation, the reflection coefficient R at the interface of a two-layer medium differing only in loss tangent is

$$R = \left|1/4\,\Delta(\tan\delta)\right|^2 \tag{9}$$

where the two layers are characterized by loss tangents of $\tan\delta$ and $\tan\delta + \Delta(\tan\delta)$, respectively.

Making use of the model of Paren and Walker (1971), they suggest that loss tangent variations of the order necessary to produce reflections may occur because of impurity distributions varying within the ice, for example, impurities either uniformly distributed or concentrated at grain boundaries, without requiring that the total concentration vary. This factor remains fairly constant with depth, making it relatively greater than the density variation at great depths, because density fluctuations are smoothed out at depth by the overburden pressure. The loss tangent effect also increases with increasing temperature, which would enhance its effect relative to density variations in the deeper, warmer layers where it is proposed as a reflection mechanism.

We have not considered this mechanism in the present analysis, since its main application, according to Paren and Robin (1975), most likely applies at a depth greater than 1500 m, which is much greater than the measured ice depth, 324 m, at Cape Folger. As well, we note the mechanism depends upon a variation in $\tan\delta$, which has not been proven to exist within the ice sheet at this location. The meltwater conductivity measurements (DC) for the Cape Folger core indicate that the fluctuation of this quantity with depth is so small as to be obscured by the measurement error and possible handling contamination (V. Morgan, personal communication).

Within the limits of these measurements, no attributable reflection exists based on conductivity changes with depth. Therefore, since density and other variations do exist and are measurably large enough to account for some of the variations in calculated and observed reflection strengths, we do not feel justified in invoking the Paren and Robin hypothesis.

Changes in inclusion geometry

This effect may be looked upon as a generalization of the density and macroscopic impurity effects where the geometry as well as the volume of the included dielectric is also considered. Evidence from the Cape Folger core indicated substantial deviation in the air bubbles from spheroids with depth, justifying an investigation into the possible effects of these geometric changes.

Some work has been done in explaining the variation of snow dielectric properties with the changing geometry of air inclusions. Evans (1965) has summarized this work, which consists primarily of attempts to explain the changes in snow dielectric properties using the empirical "Formzahl" concept first postulated by Weiner (1910). This approach is characteristic of the earlier work in heterogeneous dielectrics, but because of its empirical basis, has certain drawbacks. More recently, van Beek (1967) has replaced these empirical formulae by a derivation based on solution of electrostatic theory for dispersed media of analytical shapes.

The behavior for dilute mixtures of varying geometries has been well verified using this formulation. Paren (unpublished Ph.D. thesis) has shown that the limited data on snow which falls somewhat beyond the "dilute" definition can also be better reconciled by a variation on this analytical approach given by Böttcher's mixing equation. In that formulation, the average value of the dielectric constant of the parent medium is replaced by the total dielectric constant of the mixture. This procedure apparently gives a better estimate of the dielectric constant at high concentrations of the dispersed medium but again is a simple variation on the analytical models which work well at low concentrations. Sweeney and Colbeck (1974) have used the theoretical formulation in analyzing wet snow measurements and have found good agreement between the experimental results and theoretical predictions when the dielectric properties of the constituents are known.

After van Beek (1967), the effective dielectric constant of a mixture with dielectric constant of the medium ϵ_1 containing a dilute mixture of particles (in our case, air or dust) with dielectric constant ϵ_2 and total volume density v_2 is

$$\epsilon = \epsilon_1 \frac{\epsilon_1 + [A_j(1 - v_2) + v_2](\epsilon_2 - \epsilon_1)}{\epsilon_1 + A_j(1 - v_2)(\epsilon_2 - \epsilon_1)} . \quad (10)$$

Here $v_2 = (\rho_{ice} - \rho_{meas})/\rho_{ice}$ and A_j is the depolarization factor which is dependent only on the physical shape of the particles, most generally, ellipsoids. After Stratton (1941),

$$A_j = \frac{1}{2} abc \int_0^\infty \frac{ds}{(a^2 + s)^{1/2}(b^2 + s)^{1/2}(c^2 + s)^{1/2}(j^2 + s)} \quad (11)$$

where $j = a, b, c$, and is the axis along which the E field is aligned. It is also required that

$$A_a + A_b + A_c = 1 \quad (12)$$

where a, b, and c are the magnitudes of the axes of the ellipsoids (x, y, z) and the equation of the ellipsoid:

$$\frac{x^2}{a^2 + s} + \frac{y^2}{b^2 + s} + \frac{z^2}{c^2 + s} = 1 \quad (13)$$

where s is a variable indicating the ellipsoid confocal with a standard ellipsoid whose equation is

$$\frac{x^2}{a^2} + \frac{y^2}{b^2} + \frac{z^2}{c^2} = 1. \quad (14)$$

For the cases considered here, the ellipsoids are assumed to be prolate spheroids, i.e., $b = c$ and $a > b$. The general expression for the depolarization factor then is

$$A_a = \frac{ab^2}{2} \int_0^\infty \frac{ds}{(s + a^2)^{3/2}(s + b^2)} . \quad (15)$$

Along the minor axis b, the depolarization factor from eq 12 is.

$$A_b = \frac{1}{2}(1 - A_a). \quad (16)$$

For the prolate spheroid case, the solution of the integral, given the ratio a/b, is [from van Beek (1967)]

$$A_a = \frac{-1}{(a/b)^2 - 1} + \frac{(a/b)}{[(a/b)^2 - 1]^{3/2}} \times$$

$$\times \ln\left\{(a/b) + [(a/b)^2 - 1]^{1/2}\right\}. \quad (17)$$

We consider four cases and now give the respective expressions for the dielectric permittivity for each case. These are obtained by solving eq 10 with the appropriate value of A_j given by eq 16 or 17.

Case 1. The incident E-field is aligned along the a-axes (long axes) of the ellipsoids (which are parallelly aligned). Then

$$\epsilon = \epsilon_a = \epsilon_1\left[1 + \frac{\nu_2(\epsilon_2 - \epsilon_1)}{\epsilon_1 + A_a(\epsilon_2 - \epsilon_1)}\right]. \quad (18)$$

Case 2. The incident E-field is aligned along the b-axes (short axes) of the ellipsoids (again all of parallel alignment):

$$\epsilon = \epsilon_b = \epsilon_1\left[1 + \frac{\nu_2(\epsilon_2 - \epsilon_1)}{\epsilon_1 + A_b(\epsilon_2 - \epsilon_1)}\right]. \quad (19)$$

Case 3. The E-field is not aligned with the ellipsoid axes (random spatial orientation of the ellipsoids):

$$\epsilon = \epsilon_{ab} = \frac{1}{3}\epsilon_a + \frac{2}{3}\epsilon_b. \quad (20)$$

Case 4. The ellipsoids are all spheres ($a = b$). For this case the value of A_a is 1/3 and the solution for the permittivity is the model solution analogous to the empirical equation from Robin et al. (1969)(eq 7).

$$\epsilon = \epsilon_s = \epsilon_1\left[1 + \frac{3\nu_2(\epsilon_2 - \epsilon_1)}{2\epsilon_1 + \epsilon_2}\right]. \quad (21)$$

For the Cape Folger case under study here, no layer was found where $|\epsilon_{ab} - \epsilon_s| > 0.0012$. The depth variations between ϵ_{ab}, ϵ_s and ϵ_a, ϵ_b are larger than this value, so it can usually be assumed $\epsilon_{ab} \simeq \epsilon_s$. Equation 20, instead of eq 21, was therefore also used to give the dielectric constant for bubbles assumed spherical as well as for randomly oriented ellipsoids.

Effect of crystal orientation changes

Recent measurements (Johari and Charette 1975) have indicated that the dielectric constant values for single and polycrystalline ice agree within ± 0.2% at measured frequencies of 35 and 60 MHz. From the experiments, however, it was determined a maximum difference of 1% between the dielectric constant perpendicular and parallel to the c-axis would remain undetected. From a theoretical argument, a possible anisotropy in dielectric constant can be postulated in the MHz range.

The frequency variation of the dielectric constant can be written as (Johari and Charette 1975)

$$\epsilon'(\omega) = \epsilon_\infty + \sum_{n=1}^{N} \frac{\Delta\epsilon_n}{1 + \omega^2\tau_n^2} \quad (22)$$

where ϵ_∞ is the dielectric constant for frequencies greater than 10^{15} Hz, and $\Delta\epsilon_n$ the contribution from, and τ_n the relaxation time of, the various polarizations, each represented by a simple Debye relaxation process. From eq 22 we see that if

$$\omega^2\tau_n^2 >> 1 \quad (23a)$$

or

$$\tau_n >> \frac{1}{\omega} \quad (23b)$$

then the contribution of the relaxation process $\Delta\epsilon_n$ to the real part of the dielectric constant $\epsilon(\omega)$ at frequency ω is essentially zero.

The inequality in eq 23 corresponds to the frequency of the relaxation $\omega_n = 1/\tau_n$:

$$\omega_n << \omega. \quad (24)$$

That is, if the frequency of interest is higher than the frequency at which the relaxation process occurs, then the relaxation process in question does not contribute to the dielectric constant at the higher frequency. For example, the well-known molecular orientation processes that occur in the kHz frequency range in ice do not contribute to the dielectric constant at 35 to 100 MHz.

The electronic polarization anisotropy that occurs in the infrared region causes a $\Delta\epsilon$ between the c-axis perpendicular and the c-axis parallel of 0.0037 at – 10°C (Johari and Charette 1975). Harrison (1973) concluded that a fractional change of $\sim 10^{-4}$ in the dielectric permittivity combined with multiple layering was sufficient to produce detectable reflections in radio-echo sounding. The theoretical change in permittivity of 0.0037 caused by crystal orientation changes could then account for the observed echoes in the megahertz region if sufficient crystal orientation change occurs in these layers. This mechanism must still be cautiously invoked since the changes in permittivity arising from crystal orientation changes are very small and still have not been verified experimentally in the frequency range at which radio-echo sounders operate.

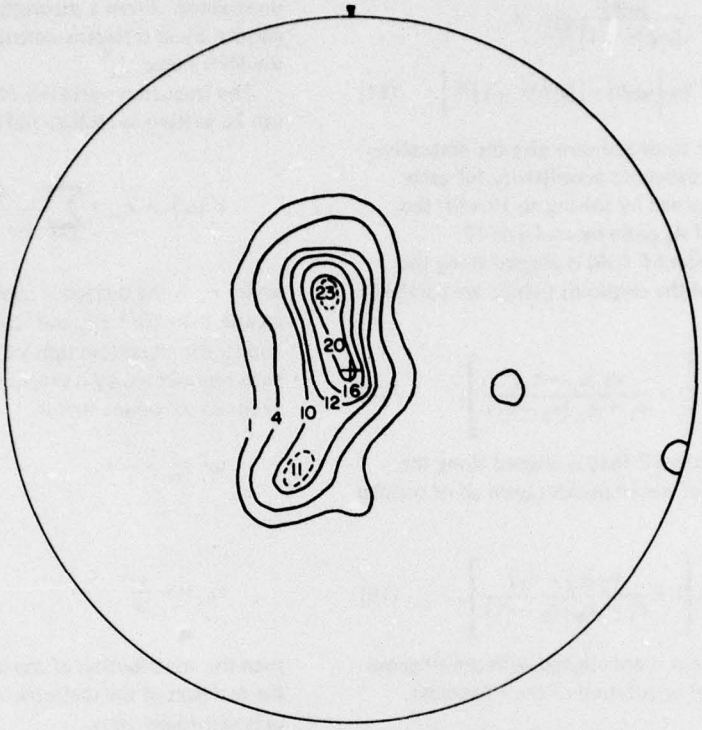

Figure 2. Fabric diagram from 171-m depth at Cape Folger.

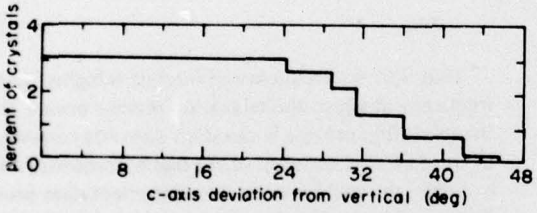

Figure 3. Distribution of c-axes from the vertical at 171-m depth obtained from the fabric diagram in Figure 2 averaged over 3° intervals.

The crystal orientation effect at a given depth on the dielectric constant can be estimated as follows (Clough 1977):

$$\epsilon(z) = \epsilon_{\perp} + \Delta\epsilon_{11\text{-}\perp} \frac{\int_{\theta}\int_{\phi} n(\theta,\phi) \sin\theta \cos\phi \, d\Omega}{\int_{\theta}\int_{\phi} d\Omega} \qquad (25)$$

where $\Delta\epsilon_{11\text{-}\perp} = 0.0037$, θ is the angle between the propagation direction and the crystal axis in the vertical, ϕ is the azimuthal angle and $d\Omega = \sin\theta d\theta d\phi$. For a first approximation, we consider only the changes in the vertical angle; i.e., we assume the crystals are uniformly distributed in a cone over the vertical angle, or $n(\theta,\phi) = n(\theta)$ only. Figure 2 gives an example of a fabric diagram from Cape Folger indicating this assumption is probably not generally valid. However, there is usually more vertical than azimuthal variation in crystal fabrics from ice cores; so the main features of the dielectric constant depth variation are probably due to vertical changes in orientation. Figure 3 shows the data from Figure 2 replotted to give the vertical *c*-axis distribution only.

PHYSICAL PROPERTIES OF THE CAPE FOLGER CORE

The data on impurity levels are based entirely on meltwater conductivities and are judged to be: (1) at such a low level that we assume the loss tangent $\tan\delta < 0.01$, at MHz or higher frequencies – i.e., the material could be considered lossless; and (2) of insufficient variation with depth to cause reflections – i.e., $\Delta \tan\delta << 0.01$. No volcanic dust or ash bands were observed in the core. Therefore, the observed reflections were assumed to originate from the dielectric effects of

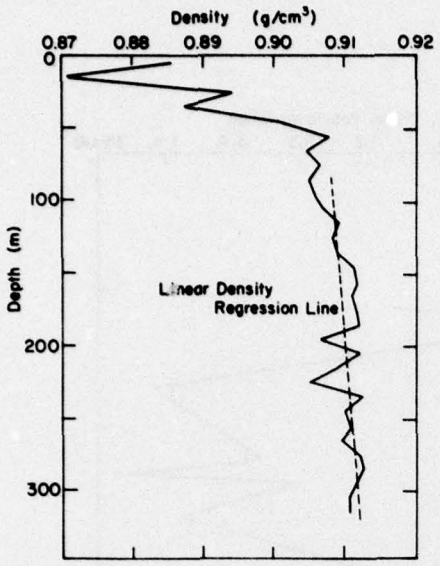

Figure 4. Variation of ice density with depth at Cape Folger and the results of a linear regression of density upon depth.

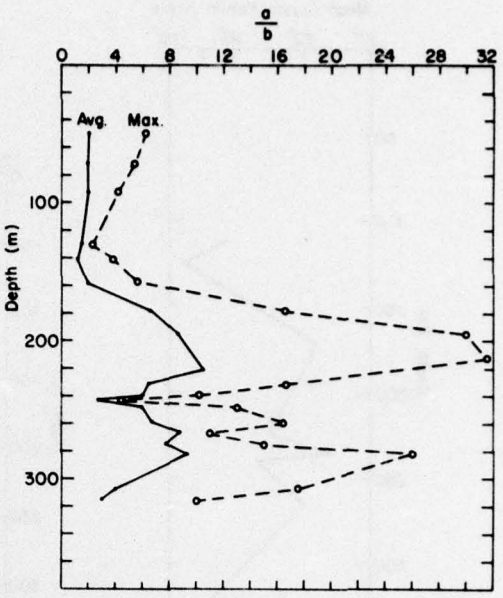

Figure 5. Variation with depth in the ratio of long axis to short axis a/b of air bubbles from the Cape Folger core. Data obtained by Matsuto (unpubl) provided by Budd (1972).

the three mechanisms discussed as follows: (i) density variations, (ii) air bubble geometry variations, and (iii) crystal orientation variations.

After discussing these physical property variations and the available radio-echo sounding data, we then give the computed dielectric constant variations based on the individual and combined physical properties.

Density-depth profile

Figure 4 indicates the variation of density with depth. The densities are quite high even in the upper parts of the profile since the core was obtained in an ablation region of the ice sheet. The density profile is obtained from 5-cm cubes taken at approximately 10-m intervals and, in some cases, the indicated density may be of uncertain value. For example, the value at 195-m depth appears to be the result of a single measurement and therefore might be in error. In contrast, the relatively low density at 225-m depth is consistent with the trends immediately above and below, so, it is believed it represents a "true" value for that point. These points cause considerable dielectric constant change and are of particular interest in the reflection coefficient calculation discussed later. For the purposes of the dielectric constant calculation, the density was obtained from the data points indicated or a linear interpolation between the points. The dielectric constant was then calculated from eq 20 and the power reflection coefficient from eqs 1, 3, 4 and 5.

Air bubble-geometry depth profile

Figure 5, based on data measured by Matsuto (unpublished), shows the variation in bubble geometry with depth measured from ice thin sections taken primarily in the horizontal plane; the figure gives both the average and maximum values of a/b. Measurements were taken at the depths indicated. As mentioned earlier, the geometry was assumed to be prolate spheroids characterized by the major and minor diameters a and b. Prolate spheroids are the conceptually simplest geometry derived from the experimental data. Figure 5 thus gives the ratio a/b as a function of depth. Budd (pers. comm.) has indicated that the portions of the core where high a/b ratios are present (below ~ 165-m depth) are also characterized by alignment of the long bubble axes, roughly in the direction of glacier flow or maximum surface slope. The dielectric constant was calculated for the four cases indicated above using the average a/b taken from Figure 5 and the density information from Figure 4. Linear interpolation between data points was made in both cases to obtain equally-spaced dielectric constant-depth profiles.

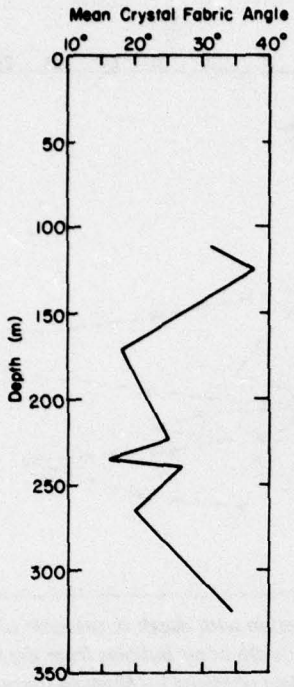

Figure 6a. First moment of the distribution

$$\bar{\theta} = \sum_{\theta=0}^{\pi/2} \theta n(\theta) \Delta\theta$$

of c-axes from the vertical.

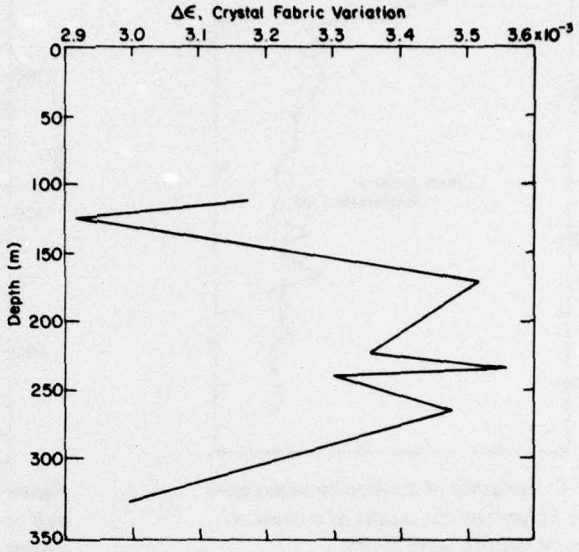

Figure 6b. Variation of the dielectric constant caused by mean crystal fabric angle variations shown in Figure 6a.

Crystal orientation-depth profile

Examples of crystal orientation data from the Cape Folger core taken from data obtained by Wakahama are given in Budd (1972). The usual presentation for ice crystal orientation data is the fabric diagram which gives the projection of the cumulative crystal orientation from a hemisphere onto a plane. An example of a fabric diagram from Cape Folger was given in Figure 2 and the derived vertical distribution in Figure 3. The first moment of the distribution (mean angle) from each depth is

$$\bar{\theta} = \sum_{\theta=0}^{\pi/2} \theta n(\theta) \Delta\theta \,. \qquad (26)$$

The variation of $\bar{\theta}$ with depth is shown in Figure 6a. The graph can then be used to compute the dielectric constant-depth variation from the following approximation to eq 25:

$$\epsilon(z) = \epsilon_{\perp} + 0.0037 \cos\bar{\theta}\,(z) \qquad (27)$$

where $\bar{\theta}$ is the mean angle at depth given in Figure 6a. The variation of $\Delta\epsilon = 0.0037 \cos\bar{\theta}$ with depth is given in Figure 6b.

As mentioned earlier, this relationship does not account for the azimuthal variation in crystal orientation; however, that quantity shows small variation for this particular core.

Radio-echo sounding data

There have been three echo sounding traverses of the Cape Folger area carried out by the Australian National Antarctic Research Expedition (ANARE): in 1967 at a frequency of 35 MHz, and in 1973 and 1975 at a frequency of 100 MHz. Unfortunately, the 1975 traverse did not take any measurements within 200 m of the core site, the core having been obtained in 1969. The bed topography appears to be so rough in the Cape Folger area that the depth determination from the 1975

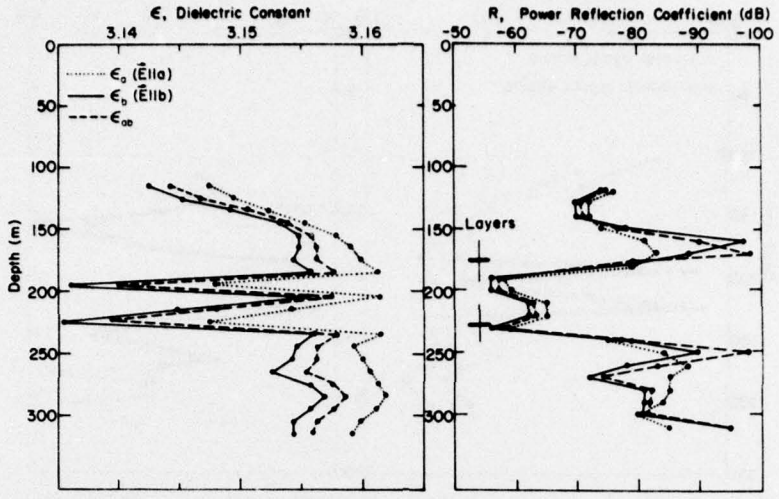

Figure 7. Dielectric constant and power reflection coefficient vs depth, including the effects of density variations, bubble elongation and orientation, and crystal fabric. The positions of the internal layers observed by radio-echo sounding are shown (+). (The amplitude of the observed echoes is unknown and their position, as shown, on the dB axis is arbitrary.)

traverse is 100 m deeper than the previous traverses. In addition, the transmitting pulse length used during this traverse was long enough to override any return echoes from depths less than 300 m. Hence, we consider only the results from the earlier work. The 1967 traverse indicated an ice depth of 345 m and two closely spaced layers at 218 and 235 m. The traverse in 1973 found an ice depth of 321 m, a strong echo at 177 m, and a weak one at 228 m.

The reasons for the differences between the two measurements are open to discussion. One possibility is the different frequencies used in the two years. If the enhancement of a return is due to an effect with an orientational character, such as bubble elongation, or crystal orientation, then the strength of the return would also depend on the relative orientations of the transmitting and receiving antennas. We will take the above work to indicate the existence of two layers at Cape Folger: one at 177 ± 15 m and a second one in the 218- to 235-m region, given by 228 ± 15 m. The ice depth from the core closely corresponds to the ice depth determined from the 1973 traverse, indicating proximity of the locations. The errors on the layer positions are based on the uncertainty in reading the travel times from the A-scan photographs of about ± 0.2 μsec, leading to a possible layer depth error of ± 15 m.

There might be some objection to using results from the above traverses in 1967 and 1973 because they were done at different frequencies. The frequency difference appears in eq 5 in the $\tanh \gamma_i d_i$ term. However, with the choice we make for d_i = 10 m, and using $\epsilon_i \approx 3.17$ in eq 3 for γ_i, $\tanh \gamma_i d_i \approx 1.0$, for either 35 MHz or 100 MHz. In this range of frequencies and for our choice of d_i, our results should therefore be frequency independent.

RESULTS AND CONCLUSIONS

As indicated previously, the only effects felt to be of importance in explaining the layering at Cape Folger are density fluctuations, bubble elongation and bubble orientation, and fluctuations in ice crystal fabric orientation. Figure 7 shows the dielectric constant and the power reflection coefficient as a function of depth including all these effects. ϵ_a is the dielectric constant with the incident E field aligned along the long axis, a, of the bubbles, ϵ_b the dielectric constant for the E field along the short axis, b, and ϵ_{ab} the dielectric constant for random bubbles. The case of purely spherical bubbles, ϵ_s, which would show just the effect of density fluctuations, has been excluded from Figure 7, since as was noted previously, it does not differ appreciably from ϵ_{ab}. The location of the internal layering from the radio-echo records is also indicated in Figure 7.

The layering is seen to be located very close to the position of the highest values of the reflection coefficient, which would be the predicted depth for enhanced

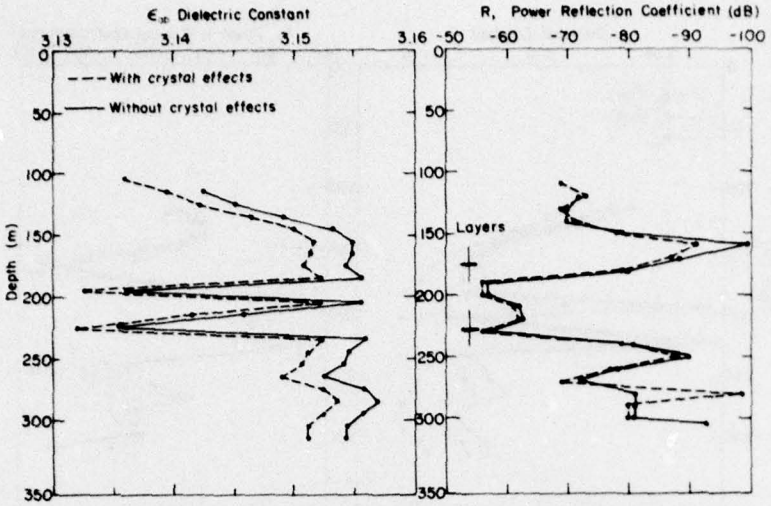

Figure 8a. The quantity ϵ_{ab} and the corresponding reflection coefficient vs depth with and without crystal effects.

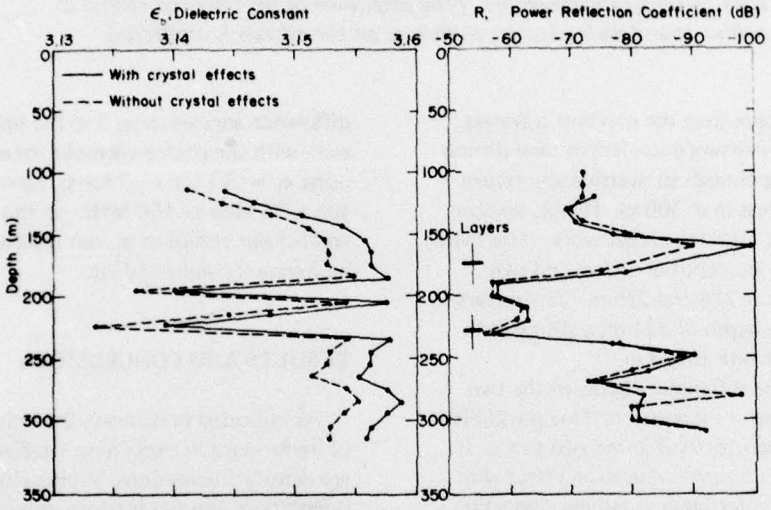

Figure 8b. The quantity ϵ_b and corresponding power reflection coefficient vs depth as in Figure 8a.

reflections. The enhanced reflections do appear to be at a slightly lower depth than the measured layering, but the data points used to calculate the permittivity were taken every 10 m, giving rise to a ± 5-m uncertainty in our calculations of the permittivities. Given the uncertainty in the echo sounding, that the internal layering differs from the region of highest reflection coefficient by only 10 or 15 m is well within the errors.

The dielectric constants in Figure 7 all display the same variation as a function of depth, though ϵ_b has the highest values of the reflection coefficient and indicates that it would yield the most enhanced return. However, the gross structure of the dielectric constant is really determined by the density fluctuations, as can be noted by recalling that ϵ_{ab} is a measure of the density effects alone and that it indicates enhanced reflections at the same locations as the other dielectric constants. While the overall structure of the reflection coefficient is determined by the density fluctuations, the bubble orientation could change the coefficient by a few dB's, with ϵ_b providing an enhancement and ϵ_a a decrease over the values for ϵ_{ab}.

Figure 7 indicates the bubble elongation and bubble orientation effects by noting the differences between ϵ_a, ϵ_b and ϵ_{ab}. Figures 8a and 8b show the crystal fabric

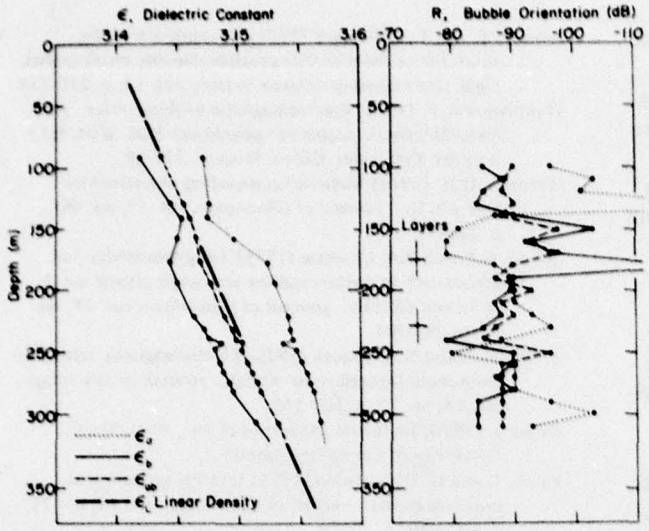

Figure 9a. The dielectric constant and reflection coefficient for the various cases of bubble configurations as a function of depth using the linear regression density.

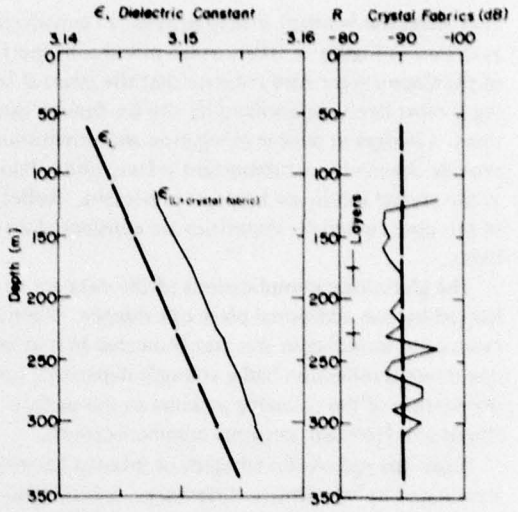

Figure 9b. The dielectric constant and reflection coefficient for crystal fabric effects as a function of depth using the linear regression density.

orientation effects. In these figures ϵ_{ab} and ϵ_b are plotted as a function of depth with and without the crystal effects; a graph of ϵ_a would indicate the same sorts of differences and so is not included. Both of the figures indicate that changes in the crystal fabrics can lead to a 1- or 2-dB change over the results without the crystal information. The inclusion of the crystal effects lowers the reflection coefficients because, in eq 27, $\epsilon_{\perp}$ is the dielectric constant without crystal effects, and any deviation of the c-axis from the horizontal increases the dielectric constant and decreases the reflection coefficient.

Figures 9a and 9b indicate further that the structure of the dielectric constant is determined by the density fluctuations. They are a result of carrying out a linear regression of the density upon depth. This results in the fit

$$\rho_L(z) = 907.1 + 0.0144z \qquad (28)$$

where $\rho_L(z)$ is the density in kg/m^3 and z is the depth in meters. This line is also plotted in Figure 4. From equation 21, this density may be used to define a "linear density" dielectric constant for spherical bubbles

$$\epsilon_L = 3.1396 + 0.000044z. \qquad (29)$$

This is plotted on Figures 9a and 9b; the reflection coefficient for ϵ_L is – 89 dB, irrespective of depth density based on a "step" change in the dielectric constant at 10-m intervals given by $\epsilon_{i+1} - \epsilon_i = 0.00044$. The other quantities in the figures are the permittivities and reflection coefficients with the inclusion of the air bubble effects (Fig. 9a) and crystal fabric effects (Fig. 9b). Without the density fluctuations, all the reflection coefficients are less than about – 79 dB and average about – 90 dB. Thus, removing the density fluctuations removes the wide variation of dielectric constants, as shown in Figure 7, and also decreases the range of high reflection coefficient from – 55 to – 60 dB to – 79 to – 90 dB in the region of the layering.

We note, however, that the calculated high reflection coefficient associated with the layer at 177 ± 15 m is based on a single density measurement at 195-m depth. If this measurement is incorrect, we see from Figure 9a that a relative peak in the reflection coefficient would still exist based on the air bubble orientation changes even when the density variation is smoothed out by a linear regression line. Although the calculated reflection coefficient is some 20 dB down from the possible density effect, it is still above – 80 dB and represents a "viable" reflection cause. Its calculated position as shown in Figure 9a also more nearly coincides with the measured position of the radio-echo layer, although given the errors on both the calculation and measurement, this may not be a significant feature.

The bubble effects give a wider range than the crystal effects, leading to the conclusion that the bubble effects would then be a more likely source for any enhancement than fabric changes, and, as shown in Figures 8a and 8b, the crystal effects actually decrease the reflection coefficient, while the bubbles aligned with their short

axes along the incident E field provide an enhancement, as shown in Figure 7. The various physical properties of the Cape Folger core indicate that the internal layering is most likely determined by the ice density fluctuations. Changes in bubble elongation and orientation provide the next most important effect, while changes in the crystal fabric are the least important. Reflections in this core caused by impurities are considered unlikely.

The glaciological implications of the data are enhanced by one additional piece of evidence. Recent radio-echo sounding in this area indicated that at least one internal reflection had a strength dependent on the orientation of the receiving antenna to the surface (Budd and Harrison, personal communication).

Since the radio-echo strength of internal layering is dominated by the density differences, features usually displaying an isotropic or non-orientational character, we must examine the available evidence to see if there is an explanation consistent with an echo caused by a change in density but also exhibiting an orientational or non-isotropic dependence. From Figures 4 and 5, it appears that the depth locations of the density variations correspond well with the most asymmetric air bubbles, an indicator of enhanced deformation at these depths. We conclude that the density variation and reflection strength therefore reflect a non-isotropic deformational horizon at this location rather than the isotropic depositional horizon usually associated with density variations alone. The deformational event may have been a surge or strong localized shear layer between rapidly moving ice and more stagnant ice. Tracking of this layering, using a deformational assumption for occurrence, may give some insight into the previous and ongoing internal mechanics of the ice sheet in this region. We also infer that the density variations observed at other locations in the ice sheet must be correlated well with deformational indicators such as air bubbles, fabrics, and possibly grain sizes before heavy reliance is placed on their use as depositional markers in interpreting the prior history of the ice sheets.

LITERATURE CITED

Budd, W.F. (1972) The development of crystal orientation fabrics in moving ice. *Zeitschrift für Gletscherkunde und Glazialgeologie*, bd. VIII, ht 1-2, p. 65-105.

Clough, J. (1977) Radio echo sounding: Reflections from internal layers in ice sheets. *Journal of Glaciology*, vol. 18, no. 78, p. 3-12.

Evans, S. (1965) Dielectric properties of ice and snow – A review. *Journal of Glaciology*, vol. 5, no. 42, p. 773-92.

Gow, A.J. and T. Williamson (1971) Volcanic ash in the antarctic ice sheet and its possible climatic implications. *Earth and Planetary Science Letters*, vol. 13, p. 210-218.

Gudmandsen, P. (1971) Electromagnetic probing of ice. In *Electromagnetic probing in geophysics* (J.R. Wait, Ed.). Boulder, Colorado: Golem Press, p. 321-38.

Harrison, D.H. (1973) Radio echo sounding of horizontal layers in ice. *Journal of Glaciology*, vol. 12, no. 66, p. 383-97.

Johari, G.P. and P.A. Charette (1975) The permittivity and attenuation in polycrystalline and single-crystal ice Ih at 35 and 60 MHz. *Journal of Glaciology*, vol. 14, no. 71, p. 293-304.

Linlor, W.I. and G.R. Jiracek (1975) Electromagnetic reflection from multi-layered snow models. *Journal of Glaciology*, vol. 14, no. 72, p. 501-516.

Paren, J. (1970) Dielectric properties of ice. Ph.D. Thesis, University of Cambridge (unpubl.).

Paren, J. and G. DeQ. Robin (1975) Internal reflection in polar ice sheets. *Journal of Glaciology*, vol. 14, no. 71, p. 251-260.

Paren, J. and J.C.F. Walker (1971) Influence of limited solubility on the electrical and mechanical properties of ice. *Nature, Physical Science*, vol. 230, no. 12, p. 77-79.

Robin, G. DeQ., S. Evans and J.R. Bailey (1969) Interpretation of radio echo sounding in polar ice sheets. *Philosophical Transactions of Royal Society*, Ser. A, vol. 265, no. 1166, p. 437-505.

Stratton, J.A. (1941) *Electromagnetic theory*. New York: McGraw Hill Book Co., Inc.

Sweeney, B.D. and S.C. Colbeck (1974) Measurements of the dielectric properties of wet snow using a microwave technique. CRREL Research Report 325. AD 001550.

van Beek, L.K.H. (1967) Dielectric behavior of heterogeneous systems. *Progress in Dielectrics*, vol. 7, p. 69-114.

Wait, J.R. (1958) Transmission and reflection of electromagnetic waves in the presence of stratified media. *Journal of Research*, National Bureau of Standards, vol. 61, no. 3, p. 205.

Weiner, O. (1910) Zur Theorie der Refraktionkonstanten Berichte über die Verhandlungen der Königlich Sachsischen Gesellschaft der Wiessenschaften zu Leipzig. *Mathematisch-Physikalische Klasse*, bd. 62, ht. 5, p. 256-68.

☆U.S. GOVERNMENT PRINTING OFFICE: 1977—702-583/19